Supplementary Material for: Micro-mechanical response and power-law exponents from the longitudinal fluctuations of F-actin solutions.

Pablo Domínguez-García
Dep. Física Interdisciplinar, Universidad Nacional de Educación a Distancia (UNED), Madrid, Spain

Jose R. Pinto
Department of Biomedical Sciences, Florida State University College of Medicine, Tallahassee, Florida, USA.

Ana Akrap and Sylvia Jeney
Department of Physics, University of Fribourg, Fribourg, Switzerland

(Dated: March 1, 2023)

In this supplemental document we include a whole set of example curves which have not been added in the main manuscript: melamine resin tracers in F-actin, F-actin/Tm complex (without Tn) and F-actin/Tm/Tn, and PS tracer in F-actin and F-actin/Tm. We include these figures here for the sake of completeness, since they are analogous to the ones already shown in the main paper. In this document, we also include some aspects of the experimental methods not detailed in the main paper, and a final table with summarizes all the averaged exponents for different F-actin solutions and tracers.

I. METHODS

To initially analyze the bead motion, we calculate three representative statistical quantities: mean square displacement (MSD), power-spectral density (PSD) and velocity autocorrelation (VAF). These statistical quantities are obtained in linear scale because our data acquisition set-up measures the movement of the trapped particle in fixed time-steps. However, the plotting of the data and the calculation of the power-law exponents need a double-axis logarithmic scale for the functions of interest. To avoid the linear representation and an excess of experimental points on the left part of the curves, we perform a logarithmic blocking of the calculated data. The blocking method divides the abscissa of the plot in equally distributed intervals in logarithmic scale, i.e., the blocks. All data points inside the block are averaged and their errors calculated [1]. The data in this work have been blocked in ten bins per decade, assuring a good representation and visualization of the experimental data. However, at very short-time scales, $t = 1\,\mu$s, the measured data are not sufficient to generate equally spaced blocked points because the lag time is $\Delta t = 1\,\mu$s. For this reason, we restricted the analysis to a minimum temporal value of $\sim 3.2\,\mu$s (-5.5 in based-10 logarithmic values).

A. 1P Microrheology

To obtain the viscoelastic modulus from a tracer bead immersed in the fluid, we have to convert the statistical quantities relation to the particle's motion into the complex modulus $G^*(\omega) = G'(\omega) + iG''(\omega)$, where $G''(\omega)$ is the loss modulus and $G'(\omega)$ is the elastic or storage modulus. The standard formalism in microrheology for this calculation is to employ the measured MSD through the Mason-Weitz (MW) approach based on the generalized Stokes-Einstein relation (GSER) [2] concurrent with Mason's approximation [3] to obtain:

$$G^*(\omega) = \frac{k_B T}{i\omega\pi a \overline{\langle \Delta r^2(\omega)\rangle}}, \tag{1}$$

where $\overline{\langle \Delta r^2(\omega)\rangle}$ is the one-side Fourier transform of the MSD. A second classic methodology for obtaining G^* is using the measured PSD of the probe and Kramers-Kronig (KK) integrals. The power-spectrum density is related to the imaginary part of the complex susceptibility, $\alpha^*(\omega) = \alpha'(\omega) + i\alpha''(\omega)$, by $\alpha''(\omega) = \omega\,\mathrm{PSD}(\omega)/4k_BT$. The real part of $\alpha(\omega)$ can be obtained by the known Kramers-Kronig expression:

$$\alpha'(\omega) = \frac{2}{\pi}\int_0^\infty \cos(\omega t)\,dt \int_0^\infty \alpha''(z)\sin(zt)\,dz. \tag{2}$$

Then, the complex modulus is calculated by $G^*(\omega) = 1/6\pi a\,\alpha^*(\omega)$. The main issue in this method is the calculation of (2), because of the high-values of the frequencies inside of the integrals, applied to a finite range of data. We evaluate eq. (2) by using the efficient Filon methods developed by Shampine for integrating oscillatory integrals [4], providing analogous results to the MW method [5].

The validity of the microrheology calculations depends on two assumptions: i) the applicability of the Stokes equation, which assumes that the bead moves in a continuum mechanical environment ($a > \xi$), and ii) the material should be in thermal equilibrium, or sufficiently close to it [6]. Any variation of these conditions will generate strange effects in the results when obtaining G^*. Besides,

in both described methodologies (MW and KK) a characteristic breakup for the elastic modulus, G', at high frequencies is observed. This behavior, which appears decades before the influence of the Nyquist frequency [7], is likely to occur because of the greater sensitivity of the cosine calculation at low values of t. Additionally, the Mason's approximation in the Mason-Weitz method uses $\alpha(s) \equiv (d \ln \mathrm{MSD}(t)/\ln t)|_{t=1/s}$, to locally expand the MSD around the frequency of interest s. As Mason commented in his work, if $\alpha \sim 1$ over a large temporal range, the estimate for the dominant $G''(\omega)$ is excellent, but $G'(\omega)$ degrades. Besides, the elastic component tends to be very sensitive to artifacts [8, 9], and great care has to be applied regarding the interpretation of the calculated elastic modulus at higher frequencies. Therefore, we limit the calculations for the elastic modulus, $G'(\omega)$, at $\omega < 10\,\mathrm{kHz}$ (already high-frequency) and we focus on the behavior of the loss modulus, $G''(\omega)$, in terms of very high-frequency microrheology of the fluid.

B. Limits of the regression analysis

Here, the values of the power-law exponents are calculated by linear regressions at logarithmic scale to the data blocked at 10 points for decade. For this calculation, we need to define a criteria for the bottom and top limits, especially in the case of the MSD, where the influence of the elastic forces at high-time values is clear. The analytical solution of Langevin equations [10] for a spherical particle immersed in a Newtonian fluid under an external harmonic potential with no-slip boundaries and hydrodynamic effects [11] depends on the following time-scales: $\tau_p = m^*/(6\pi\eta a)$, $\tau_f = \rho_f a^2/\eta$, and $\tau_k = 6\pi\eta a/k$, where a is the bead radius, η is the fluid's viscosity and ρ_f its density. The effective mass $m^* \equiv m_p + m_f/2$ appears because of the influence of hydrodynamics, with m_f the mass of the displaced fluid and m_p de mass of the particle, The time-scale τ_p is an inertial time scale describing the moment relaxation because of friction forces, τ_f represents the time needed by the fluid vortex to propagate itself over one particle radius, and τ_k is the temporal scale where the restoring force of elastic constant (trap stiffness), k, is predominant. These characteristic times verify $\tau_p < \tau_f < \tau_k$ for Newtonian fluids, but the analogous expressions for a power-law fluid depend on unknown parameters related to viscosity of the medium and the friction memory kernel [12].

The experimental time limits are, therefore, calculated empirically, according to the general behavior of the calculated statistical quantities, by adding multiplying factors to the Newtonian time scales, τ_k and τ_f. Then, we define the top limit for the MSD as $f_k\,\tau_k$, while the bottom limit is $f_f\,\tau_f$. The f_f factor is fixed to $f_f = 5$ because of the position of the minimum in the $|\mathrm{VAF}|(t)$ in the first zero-crossing value. The factor related to $\tau_k = 6\pi\eta a/k$ is also set to $f_k = 5$, to perform the linear regression far enough from the influence of the elastic plateau. The k value has to be modified for taking into account not only the contribution from the optical trap, but also the elastic component of the fluid. The elastic modulus for this fluid is estimated to be $G^0 \sim 1\,\mathrm{Pa}$ (see section I A), hence $k \approx k_i + 6\pi a G^0$, where k_i is the applied trap stiffness ($i = 1 \cdots 4$). The corresponding limits applied to the PSD(f) and the loss modulus $G''(\omega)$ (section I A) are $\omega_f = 2\pi/(f_f\,\tau_f)$ and $\omega_k = 2\pi/(f_k\,\tau_k)$. For the $|\mathrm{VAF}|(t)$, the short-time limit is the same: $f_f\,\tau_f$. The determination of the top limit value, $f_k\,\tau_k$, is set by using $f_k = 0.03$.

C. Calibration of example curves

One main issue analyzing OTI data is how to convert the measured signals to units of displacements of the trapped-Brownian beads, i.e., how to calibrate and obtain the volts-to-meter conversion factor. This calibration is straightforward when the bead is immersed in Newtonian fluids [13–15]; if the mechanical behavior of the fluid is simple, like a Kevin-Voigt fluid [5]; or by using the method of the double flow chamber [16, 17]. Classic methods are comparing with the MSD characteristic plateau at long-times, $\mathrm{MSD}(\infty) = 2k_BT/k$, if the optical trap stiffness is already known, or using the Lorentzian form of the PSD [18].

One calibration method in non-Newtonian fluids uses the averaged values of $\langle k \rangle$ measured in water, in analogy with the double flow chamber method [19]. Then, the low-frequency elastic modulus of the fluid should be greater than the elastic component from the optical trap, i.e., $G'(0) > G'_k = k/6\pi a$. If not, the optical trap may modify the fluid itself and this calibration method is not correct [20]. In other words, if the trap stiffness generates an elastic component in the order of the storage modulus of the fluid, the microrheological measurements for G' at low frequencies are not representative of the surrounding medium. As we have already analyzed in this paper, we assume that $G'(\omega_0) < 1\,\mathrm{Pa}$ for F-actin solutions at $1\,\mathrm{mg/ml}$.

With our optical tweezers, particles with $a = 0.99\,\mu\mathrm{m}$ generate $G_k = 18\,\mathrm{Pa}$ for the strongest forces ($G_k = 7\,\mathrm{Pa}$ for $a = 1.47\,\mu\mathrm{m}$). Therefore, the elastic modulus plateau measured in the fluid, when using the strongest trap, appears because of the external force. This is why calibration can be made using the averaged water value for that optical force. Conversely, the lower values of G_k are in the order of the expected values for G^0 in these F-actin solutions, in agreement with the fact that the bead could be moved inside the formed fluid using the optical tweezers in any performed experiment.

All the example curves shown here have been calibrated following these steps: i) GSER is calculated from the MSDs, and a calibration factor for the curve with the strongest optical trap (k_1) is obtained by comparing it with its G_k value measured in water; ii) if we assume that the bead is in thermal equilibrium and that

TABLE 1S: All averages of the power-law exponents for all optical forces. The parentheses in the numbers are concise notation for the numerical value of the standard uncertainty.

Material	Bead	$a(\mu\text{m})$	$k(\mu\text{N/m})$	$\langle\alpha_{\text{MSD}}\rangle$	$\langle\alpha_{\text{PSD}}\rangle$	$\langle\alpha_{\text{GSER}}\rangle$	$\langle\alpha_{\text{KK}}\rangle$	$\langle\beta_{\text{VAF}}\rangle$
Actin	PS(BSA)	0.99	9 ± 4	0.873(11)	0.869(13)	0.883(9)	0.857(13)	0.90(4)
Actin	PS (BSA)	0.99	23 ± 3	0.861(6)	0.848(7)	0.874(6)	0.851(8)	0.885(16)
Actin	PS (BSA)	0.99	85 ± 17	0.843(8)	0.836(10)	0.866(7)	0.864(9)	0.811(23)
Actin	PS (BSA)	0.99	330 ± 140	0.81(4)	0.80(4)	0.83(4)	0.855(16)	0.89(7)
Actin Tm.	PS (BSA)	0.99	9 ± 4	0.879(2)	0.875(3)	0.888(2)	0.862(3)	0.884(12)
Actin Tm.	PS (BSA)	0.99	23 ± 3	0.862(6)	0.847(6)	0.876(6)	0.854(4)	0.84(3)
Actin Tm.	PS (BSA)	0.99	85 ± 17	0.86(3)	0.85(3)	0.876(15)	0.871(17)	0.80(3)
Actin Tm.	PS (BSA)	0.99	330 ± 140	0.807(13)	0.79(3)	0.845(9)	0.853(12)	0.88(5)
Actin Tm. Tn.	PS (BSA)	0.99	9 ± 4	0.888(3)	0.877(4)	0.887(2)	0.858(7)	0.91(2)
Actin Tm. Tn.	PS (BSA)	0.99	23 ± 3	0.875(1)	0.867(3)	0.885(1)	0.865(1)	0.879(14)
Actin Tm. Tn.	PS (BSA)	0.99	85 ± 17	0.86(2)	0.856(3)	0.878(13)	0.875(4)	0.81(3)
Actin Tm. Tn.	PS (BSA)	0.99	330 ± 140	0.839(10)	0.836(17)	0.862(7)	0.868(5)	0.82(4)
Actin	Resin	1.47	7 ± 2	0.81(3)	0.81(2)	0.82(4)	0.782(19)	1.09(7)
Actin	Resin	1.47	13 ± 3	0.816(16)	0.808(15)	0.829(18)	0.790(17)	1.08(7)
Actin	Resin	1.47	42 ± 5	0.81(3)	0.81(3)	0.82(3)	0.80(3)	1.05(7)
Actin	Resin	1.47	180 ± 70	0.79(3)	0.80(3)	0.80(4)	0.82(4)	1.05(8)
Actin Tm.	Resin	1.47	7 ± 2	0.815(13)	0.806(13)	0.827(12)	0.781(12)	1.06(4)
Actin Tm.	Resin	1.47	13 ± 3	0.824(7)	0.815(7)	0.837(7)	0.795(1)	1.010(16)
Actin Tm.	Resin	1.47	42 ± 5	0.814(11)	0.808(8)	0.829(13)	0.801(13)	1.00(5)
Actin Tm.	Resin	1.47	180 ± 70	0.803(11)	0.803(13)	0.819(14)	0.822(16)	0.97(4)
Actin Tm. Tn.	Resin	1.47	7 ± 2	0.837(12)	0.827(15)	0.847(10)	0.808(9)	1.02(3)
Actin Tm. Tn.	Resin	1.47	13 ± 3	0.83(2)	0.82(2)	0.844(18)	0.806(18)	1.01(4)
Actin Tm. Tn.	Resin	1.47	42 ± 5	0.819(13)	0.813(14)	0.832(13)	0.806(18)	1.01(3)
Actin Tm. Tn.	Resin	1.47	180 ± 70	0.76(3)	0.784(2)	0.76(5)	0.802(12)	1.053(3)

the short-time bevahior reflects the polymeric structure, all curves should collapse at very short-time values [19], thus we can calculate a calibration factor for the other optical forces, iii) the PSD and VAFs are calibrated using these factors, and iv) finally, the microrheological quantities are calculated once again.

We have to emphasize that calibration is not a key factor in this study for the following reasons: the quantitative differences of 1P microrheology with bulk rheology and two-particle microrheology, the influence of the optical trap even at low trap stiffness, and because our main objective is to investigate the power-law behavior of the statistical and microrheological quantities, calculation which does not depend on the absolute values of the statistical or microrheological quantities.

Next, we give some additional experimental values for the elastic modulus at low frequencies which have been reported in the literature: $G'(\omega_0) \sim 0.1\,\text{Pa}$, with a magnetically drive rotation disk rheometer [21]; a range $0.1-10\,\text{Pa}$ for concentrations between $0.5-2.0\,\text{mg/ml}$ using 1P microrheology with DWS [22]; $G'(\omega_0) < 0.1\,\text{Pa}$ for $a = 0.24\,\mu\text{m}$ with 2P microrheology [23]; $0.1-0.2\,\text{Pa}$ using micro and macrorheometry [24]; $G'(\omega_0) \sim 0.1\,\text{Pa}$ by means of a rotation disk rheometer [25]; $G'(\omega_0) \sim 0.2\,\text{Pa}$ for 1P and 2P microrheology [26, 27]; $G'(\omega = 0.01\,\text{Hz}) = 0.1\,\text{Pa}$ [28]; $G'(\omega_0) < 0.1\,\text{Pa}$ in the cardiac thin filaments with calcium with $1\,\text{mg/ml}$ actin concentration [29]; $G'(\omega_0) < 1\,\text{Pa}$ using microrheology for different tracer bead diameters [30]; $G'(\omega_0) < 0.5\,\text{Pa}$ through a cone and plate rheometer [31].

II. RESULTS

As it has been described in the text, the entanglement length is particularly important in this study. Some experimental values for the entanglement length in the literature are the following: $l_e \sim 0.4\,\mu\text{m}$ for $24\,\mu\text{M}$ of actin (or $l_e \sim 1\,\mu\text{m}$ if this value doubles the tube diameter) [32], $l_e \sim 2.2\,\mu\text{m}$ using a plateau modulus of $G' \sim 0.1-0.2\,\text{Pa}$ for F-actin at $1\,\text{mg/ml}$ (similar to our experiments) [18], and $l_e \sim 1\,\mu\text{m}$ for F-actin at $0.3\,\text{mg/ml}$ [33].

In Table 1S, we summarize all the averaged values for the power-law exponents, including the exponent β from the VAF, for the different experiments performed in F-actin, F-actin/Tm, and F-actin/Tm/Tn. In this table, we can clearly see how β (last column) does not depend on the optical trap, only on the type of trapped particle.

The 7/8 value of the power-law exponent has been previously detected in similar F-actin experiments. Specifically, some values are the following: $\alpha = 0.86 \pm 0.04$ was obtained by diffusing wave spectroscopy (DWS) for PS BSA-coated particles with $a = 1.6\,\mu\text{m}$ and actin concentration $c_A = 0.8\,\text{mg/ml}$ [34]; $1 > \alpha > 3/4$ for silica spheres with radii $a = 0.6\,\mu\text{m}$ in $1\,\text{mg/ml}$ non-crosslinked F-actin solutions [27]; $\alpha \sim 0.9$ for entangled F-actin solution using interferometric microrheology with two optically-trapped particles [35]; $\alpha = 0.88 \pm 0.04$ in cardiac thin filaments with added calcium at $3.66\,\mu\text{M}$ with PS $0.489\,\mu\text{m}$ tracers [29]; a 7/8 value for $G''(\omega)$ in optically trapped silica beads of $a = 2.5\,\mu\text{m}$ at $0.1\,\text{mg/ml}$ concentration [36]; 7/8 exponent for a trapped melanine

resin bead of $a = 1.5\,\mu$m at $0.5\,$mg/ml [37]; and an exponent apparently in the range $1 > \alpha > 3/4$ for $G''(\omega)$ using one-point microrheology of a collection of bead sizes for $c_A = 1\,$mg/ml [38].

In the following pages we include the example curves of F-actin solutions which have been not shown in the main manuscript.

[1] H. Flyvbjerg and H. G. Petersen, J. Chem. Phys. **91**, 461 (1989).
[2] T. G. Mason, K. Ganesan, J. H. van Zanten, D. Wirtz, and S. C. Kuo, Phys. Rev. Lett. **79**, 3282 (1997).
[3] T. G. Mason, Rheol. Acta **39**, 371 (2000).
[4] L. F. Shampine, Appl Math Comput. **221**, 691 (2013).
[5] P. Domínguez-García, G. Dietler, L. Forró, and S. Jeney, Soft Matter **20**, 4234 (2020).
[6] E. M. Furst and T. M. Squires, *Microrheology* (OUP Oxford, 2017).
[7] K. Nishi, M. L. Kilfoil, C. F. Schmidt, and F. C. MacKintosh, Soft Matter **14**, 3716 (2018).
[8] T. Savin and P. S. Doyle, Phys. Rev. E **76**, 021501 (2007).
[9] P. Domínguez-García and M. A. Rubio, Appl. Phys. Lett. **102**, 074101 (2013).
[10] Langevin, P., C.R. Acad. Sci. Paris **146**, 530 (1908).
[11] Clercx, H. J. H. and Schram, P. P. J. M., Phys. Rev. A **46**, 1942 (1992).
[12] D. S. Grebenkov, Phys. Rev. E **83**, 061117 (2011).
[13] M. Grimm, T. Franosch, and S. Jeney, Phys. Rev. E **86**, 021912 (2012).
[14] A. Butykai, F. M. Mor, R. Gaál, P. Domínguez-García, L. Forró, and J. S., Comput. Phys. Commun. **196**, 599 (2015).
[15] A. Butykai, P. Domínguez-García, F. M. Mor, R. Gaál, L. Forró, and J. S., Comput. Phys. Commun. **220**, 507 (2017).
[16] E. Bertseva, D. Grebenkov, P. Schmidhauser, S. Gribkova, S. Jeney, and L. Forr, Europhys. J. E. Soft. Matter. **35**, 1 (2012).
[17] P. Domínguez-García, F. Cardinaux, E. Bertseva, L. Forró, F. Scheffold, and S. Jeney, Phys. Rev. E **90**, 060301 (2014).
[18] K. M. Addas, C. F. Schmidt, and J. X. Tang, Phys. Rev. E **70**, 021503 (2004).
[19] P. Domínguez-García, L. Forró, and S. Jeney, Appl. Phys. Lett. **109**, 143702 (2016).
[20] M. Tassieri, Soft Matter **11**, 5792 (2015).
[21] B. Hinner, M. Tempel, E. Sackmann, K. Kroy, and E. Frey, Phys. Rev. Lett. **81**, 2614 (1998).
[22] T. Gisler and D. A. Weitz, Phys. Rev. Lett. **82**, 1606 (1999).
[23] J. C. Crocker, M. T. Valentine, E. R. Weeks, T. Gisler, P. D. Kaplan, A. G. Yodh, and D. A. Weitz, Phys. Rev. Lett. **85**, 888 (2000).
[24] F. G. Schmidt, B. Hinner, and E. Sackmann, Phys. Rev. E **61**, 5646 (2000).
[25] W. H. Goldmann, Biochem. Biophys. Res. Commun. **276**, 1225 (2000).
[26] M. L. Gardel, M. T. Valentine, J. C. Crocker, A. R. Bausch, and D. A. Weitz, Phys. Rev. Lett. **91**, 158302 (2003).
[27] G. H. Koenderink, M. Atakhorrami, F. C. MacKintosh, and C. F. Schmidt, Phys. Rev. Lett. **96**, 138307 (2006).
[28] M. L. Gardel, K. E. Kasza, C. P. Brangwynne, J. Liu, and W. D. A., Methods Cell Biol. **89**, 487 (2008).
[29] M. Tassieri, R. M. Evans, L. Barbu-Tudoran, J. Trinick, and T. A. Waigh, Biophys. J. **94**, 2170 (2008).
[30] J. He and J. X. Tang, Phys. Rev. E **83**, 041902 (2011).
[31] G. H. Koenderink, Z. Dogic, F. Nakamura, P. M. Bendix, F. C. MacKintosh, J. H. Hartwig, T. P. Stossel, and D. A. Weitz, Proc. Natl. Acad. Sci. USA. **106**, 15192 (2009).
[32] A. Palmer, T. G. Mason, J. Xu, S. C. Kuo, and D. Wirtz, Biophys. J. **76**, 1063 (1999).
[33] H. Isambert and A. C. Maggs, Magnetohydrodynamics **29**, 1036 (1996).
[34] B. A. Chae and M. F. Furst, Langmuir , 3084 (2005).
[35] M. Atakhorrami, D. Mizuno, G. H. Koenderink, T. B. Liverpool, F. C. MacKintosh, and C. F. Schmidt, Phys. Rev. E **77**, 061508 (2008).
[36] M. Tassieri, R. M. L. Evans, R. L. Warren, N. J. Bailey, and J. M. Cooper, New J. Phys. **14**, 115032 (2012).
[37] D. S. Grebenkov, M. Vahabi, E. Bertseva, L. Forró, and S. Jeney, Phys. Rev. E **88**, 040701 (2013).
[38] M. Atakhorrami, G. H. Koenderink, J. F. Palierne, F. C. MacKintosh, and C. F. Schmidt, Phys. Rev. Lett. **112**, 088101 (2014).

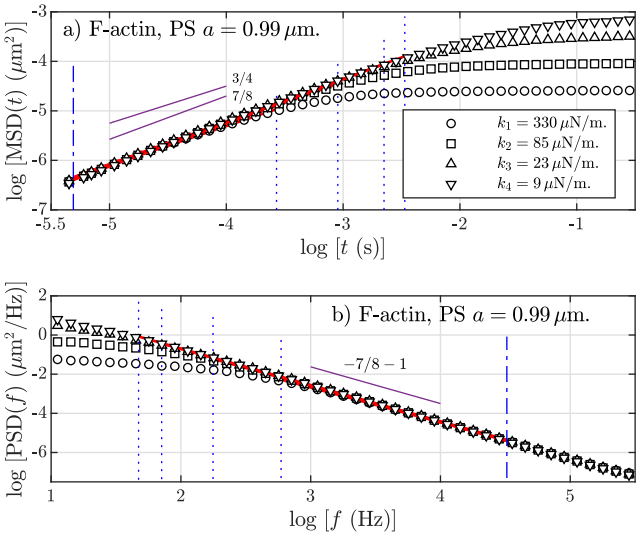

FIG. 1S: (Color online) a) One dimensional mean-squared displacement (MSD) and b) Power spectral density (PSD) for 1 mg/ml F-actin solution for an optically trapped polystyrene (PS) BSA-added tracer with $a = 0.99\,\mu$m. All the experimental data have been blocked in 10 bins per decade. Errors are negligible, not plotted for clarity. Trapping forces are indicated in the legend. Regression lines (——) are calculated under the limits defined by the blue dashed lines: top (·····) and lower limits (- - -) for the MSD (a), inversely for the PSD (b). The purple line (——) is a guide for the eye indicating the power-law exponent $\alpha = 7/8$.

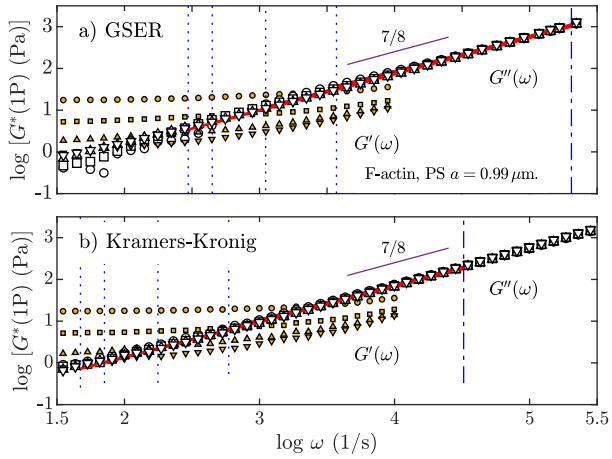

FIG. 2S: (Color online) Real (storage modulus, $G'(\omega)$, smaller points) and imaginary (loss modulus, $G''(\omega)$) parts of the complex modulus, $G^*(\omega)$, for an optically trapped polystyrene (PS) BSA-added tracer with $a = 0.99\,\mu$m in 1 mg/ml F-actin solution. a) Obtained by means of the GSER and the MSD, or b) through the Kramers-Kronig expression. Symbols and lines are the same as in Fig. 1S.

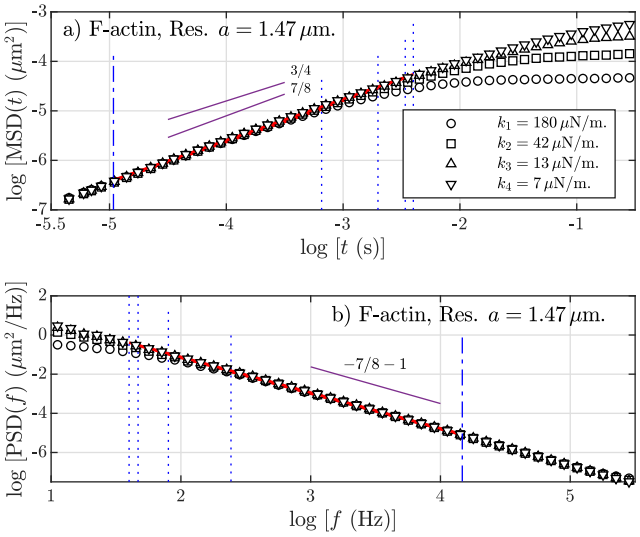

FIG. 3S: a) One dimensional mean-squared displacement (MSD) and b) Power spectral density (PSD) for 1 mg/ml F-actin solution for an optically trapped melamine resin microparticle with $a = 1.47\,\mu$m. All the experimental data have been blocked in 10 bins per decade. Errors are very small and are not plotted for clarity. Trap forces are indicated in the legend. Regression lines (——) are calculated under the limits defined by the blue dashed lines: top (·····) and lower limits (– – –) for the MSD (a), inversely for the PSD (b). The purple line (——) is a guide for the eye indicating the power-law exponent $\alpha = 7/8$.

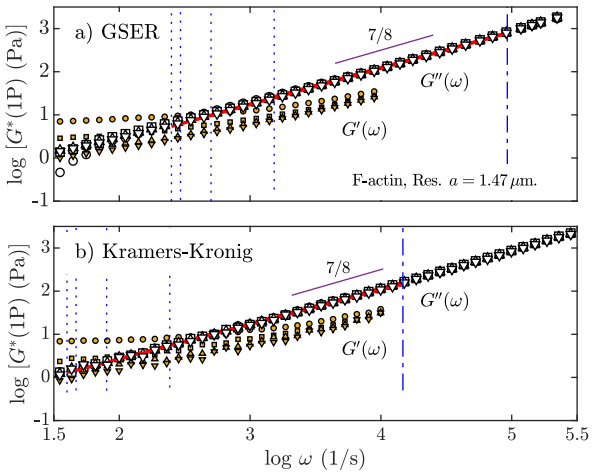

FIG. 4S: Real (storage modulus, $G'(\omega)$, smaller points) and imaginary (loss modulus, $G''(\omega)$) parts of the complex modulus ($G^*(\omega)$) for an optically trapped polystyrene (PS) melamine resin microparticle with $a = 1.47\,\mu$m in 1 mg/ml F-actin solution. a) Obtained by means of the GSER and the MSD, or b) through the Kramers-Kronig expression. Symbols and lines are the same as in Fig. 3S.

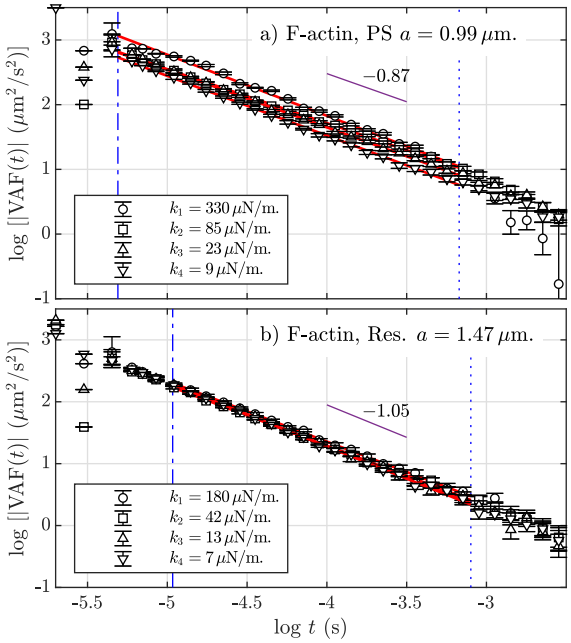

FIG. 5S: (Color online) Absolute values of the velocity autocorrelation function, |VAF| at 1 mg/ml F-actin solution for a) polystyrene (PS) BSA microparticle with $a = 0.99\,\mu$m. and b) melamine resin with $a = 1.47\,\mu$m. The errors are calculated by the blocking method. Data points for the different trap stiffnesses are indicated in the legends. Regression lines (——) are calculated under the limits defined by the blue dashed lines: top (·····) and lower limits (– · –). The purple lines (——) is a guide for the eye indicating the averaged power-law exponent β in each case.).

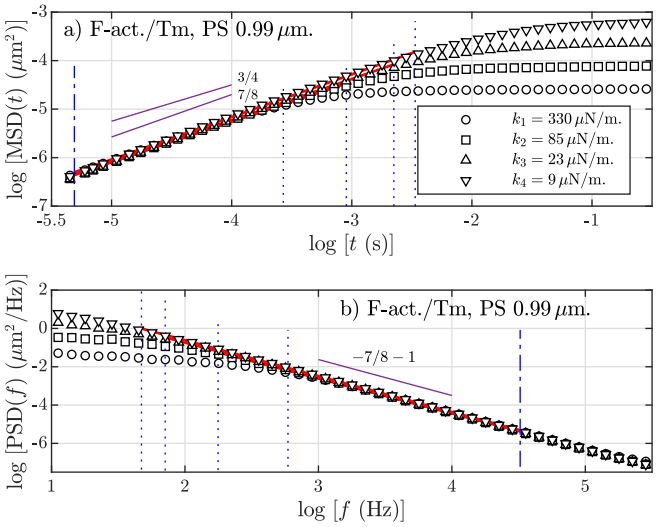

FIG. 6S: a) One dimensional particle mean-squared displacement (MSD) and b) Power spectral density (PSD) for 1 mg/ml F-Actin/Tm solution for an optically trapped polystyrene (PS) BSA microparticle with $a = 0.99\,\mu$m. The data have been blocked in 10 bins per decade. Errors are very small and are not plotted for clarity. Trap forces are indicated in the legend. Regression lines (——) are calculated under the limits defined by the dashed lines, the purple line (——) is a guide for the eye indicating the power-law exponent $\alpha = 7/8$.

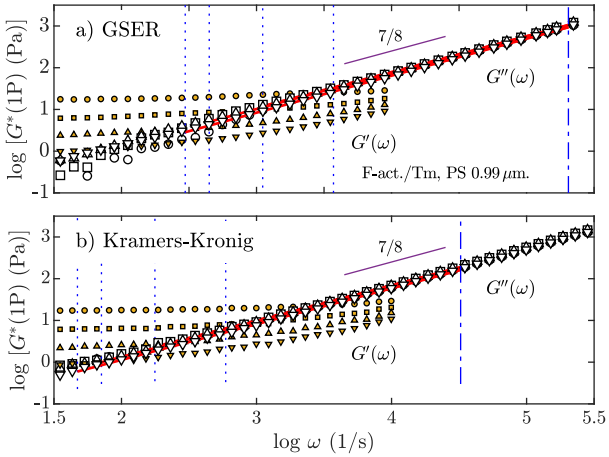

FIG. 7S: $G'(\omega)$ (small points) and $G''(\omega)$ for an optically trapped polystyrene (PS) BSA microparticle with $a = 0.99\,\mu$m in F-actin/Tm/Tn complex ($c_A = 1\,$mg/ml). a) From GSER (MW) and b) Kramers-Kronig expression. The optical forces are the same as in Fig. 6S.

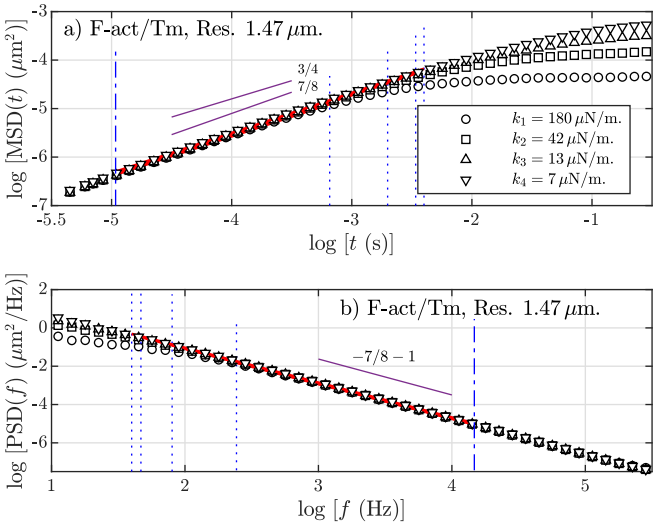

FIG. 8S: a) One dimensional particle mean-squared displacement (MSD) and b) Power spectral density (PSD) for 1 mg/ml F-Actin/Tm solution for an optically trapped melamine resin microparticle with $a = 1.47\,\mu$m. The data have been blocked in 10 bins per decade. Errors are very small and are not plotted for clarity. Trap forces are indicated in the legend. Regression lines (——) are calculated under the limits defined by the dashed lines, the purple line (——) is a guide for the eye indicating the power-law exponent $\alpha = 7/8$.

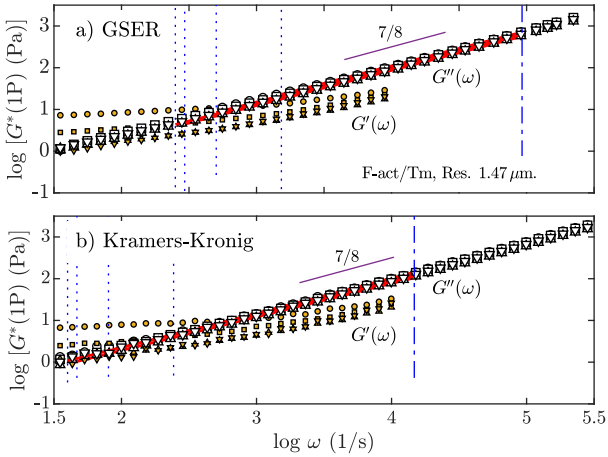

FIG. 9S: $G'(\omega)$ (small points) and $G''(\omega)$ for an optically trapped melamine resin microparticle with $a = 1.47\,\mu$m in F-actin/Tm complex ($c_A = 1\,$mg/ml). a) From GSER (MW) and b) Kramers-Kronig expression. The optical forces are the same as in Fig. 8S.

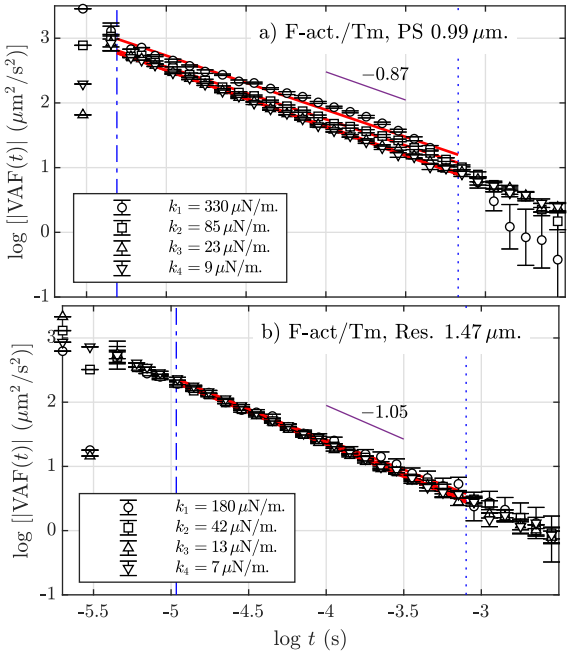

FIG. 10S: Absolute values of the velocity autocorrelation function, |VAF| at 1 mg/ml F-Actin/Tm solution for a) polystyrene (PS) BSA microparticle with $a = 0.99\,\mu$m, and b) melamine resin with $a = 1.47\,\mu$m. The errors are calculated by the blocking method. Data points for the different trap stiffnesses are indicated in the legends. Regression lines (——) are calculated under the limits defined by the blue dashed lines: top (·····) and lower limits (- - -). The purple lines (——) are a guide for the eye indicating the averaged power-law exponent β in each case.

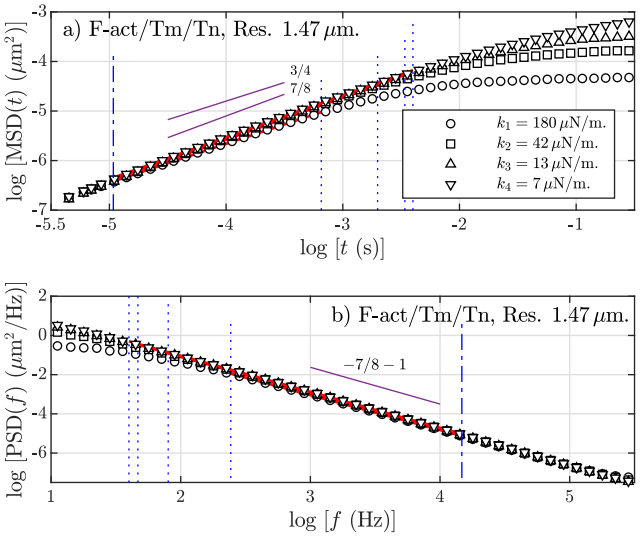

FIG. 11S: (Color online) a) One dimensional particle mean-squared displacement (MSD) and b) Power spectral density (PSD) for 1 mg/ml F-actin solution with Tm and Tn for an optically trapped melamine resin microparticle with $a = 1.47\,\mu$m.

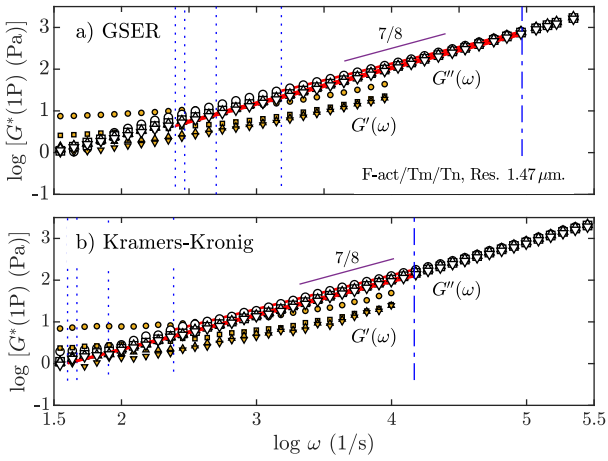

FIG. 12S: (Color online) $G'(\omega)$ (small points) and $G''(\omega)$ for an optically trapped melamine resin microparticle with $a = 1.47\,\mu$m in F-actin/Tm/Tn complex ($c_A = 1$ mg/ml). a) From GSER (MW) and b) Kramers-Kronig expression. The data symbols are the same as in Fig. 11S.